ROLE OF THE DEFORMATION SPACE ADMITTED IN THE ANALYSIS OF SPONTANEOUS FISSION*

R. SMOLAŃCZUK

Soltan Institute for Nuclear Studies
Hoza 69, PL-00-681 Warszawa, Poland
and
GSI, D-6100 Darmstadt, Germany

H.V. KLAPDOR-KLEINGROTHAUS

Max-Planck-Institut für Kernphysik
D-6900 Heidelberg, Germany

AND

A. SOBICZEWSKI

Soltan Institute for Nuclear Studies
Hoza 69, PL-00-681 Warszawa, Poland
and
GSI, D-6100 Darmstadt, Germany

(Received February 12, 1993)

Dedicated to Janusz Dąbrowski in honour of his 65th birthday

Role of the dimension of the deformation space admitted in the analysis of the spontaneous-fission half-life is studied by the example of even-even heavy nucleus $^{260}106$. Importance of taking sufficiently large dimension is demonstrated.

PACS numbers: 25.85. Ca

* Supported by the Polish State Committee for Scientific Research, grant no. 209549101, Polish–German Cooperation, grant no. X081.11, and by GSI-Darmstadt.

1. Introduction

It is well known that shell effects play essential role in the properties of nuclei. The effects are particularly strong in the magic spherical nuclei. They are, however, also large in deformed nuclei. For example, they increase the binding energy of heavy nuclei by up to about 5 MeV [1], as will be illustrated below. The property which displays especially large shell effects is the spontaneous-fission lifetime. These effects elongate the lifetime of heavy nuclei by up to about 15 orders of magnitude. This means that some of the heaviest nuclei could not exist without these effects.

To describe theoretically the large shell effects in deformed nuclei, one needs, however, to use sufficiently large deformation space. For example, it has been shown in the analysis of the ground-state energy of heavy nuclei [2, 3] that the deformations of higher multipolarity λ (up to $\lambda = 8$) give a significant contribution to this energy.

The objective of the present paper is to study the role of the deformations of higher multipolarity in the description of the spontaneous-fission lifetime of a heavy nucleus. A detailed analysis is performed for the nucleus $^{260}106$, which is the heaviest even-even nucleus, for which the spontaneous-fission lifetime has been measured. A part of the results of the analysis has been presented in [4].

2. Illustration of shell effects

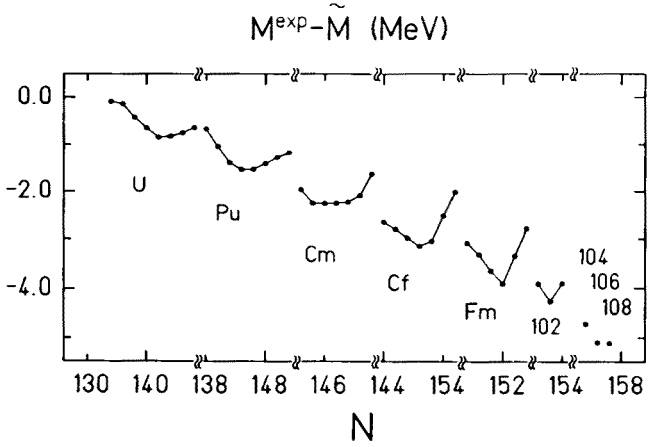

Fig. 1. Shell effects in the mass of nuclei.

Fig. 1 illustrates [1] shell effects in the mass of even-even nuclei, $M^{\exp} - \widetilde{M}$. Here, $M^{\exp}$ is the experimental mass and $\widetilde{M}$ is the mass calculated by the

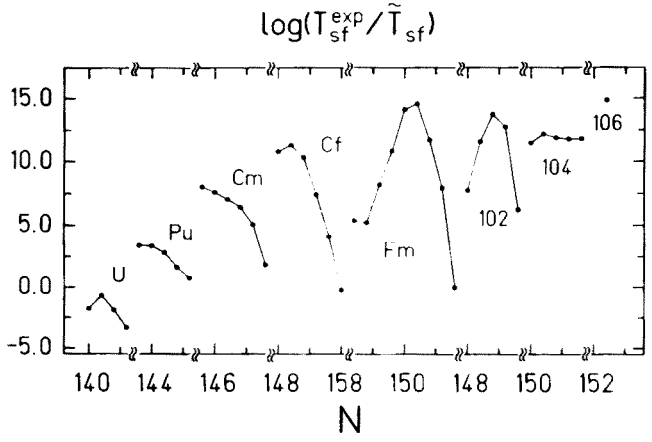

Fig. 2. Shell effects in the spontaneous-fission half-lives.

macroscopic model without any shell effects [5]. One can see that the shell effect is negative, *i.e.* it decreases masses of the nuclei. Its absolute value increases with the increasing atomic number Z, up to about 5 MeV for the heaviest known even-even nuclei: $^{260}106$ and $^{264}108$. Shell effects in the spontaneous-fission half-life T_{sf} are shown in Fig. 2 [1]. One can see that the effects delay the fission process in all heavy nuclei, except only few lightest ones (isotopes of uranium). The delay increases from few orders (Pu isotopes) to about 15 orders of magnitude for the heaviest even-even nucleus with measured T_{sf} ($^{260}106$). For such a heavy nucleus like $^{260}106$, with T_{sf} of the order of few milliseconds, this elongation makes up practically the whole half-life of these nuclei. In other words, they would not exist without shell effects. The reason is that only shell effects create the fission barrier for them.

3. Description of the calculations

The calculations are, in many aspects, similar to those of Ref. [3], where many details can be found.

3.1. Potential energy

The potential energy of the nucleus is calculated by the macroscopic-microscopic method. The Yukawa-plus-exponential model [5] with the standard values of its parameters (*e.g.* [6]) is used for the macroscopic part of the energy. The Strutinski shell correction, based on the Woods–Saxon single-particle potential [7], is taken for the microscopic part. The "universal" variant of the parameters of the potential is chosen (the same as in [3] where they are also specified).

The residual pairing interaction is treated in the usual BCS approximation. The strength of the interaction is taken the same as in [3], where it has been fitted to recent data for nuclear masses.

3.2. Inertia tensor

The inertia tensor describes the inertia of a nucleus with respect to changes of its deformation. We calculate it in the cranking approximation. The corresponding formula is (*e.g.* [8–13])

$$B_{\alpha_i\alpha_j} = 2\hbar^2 \sum_{\nu\nu'} \frac{\langle\nu|\frac{\partial H}{\partial\alpha_i}|\nu'\rangle\langle\nu'|\frac{\partial H}{\partial\alpha_j}|\nu\rangle}{(E_\nu + E_{\nu'})^3}(u_\nu v_{\nu'} + u_{\nu'} v_\nu)^2 + P^{ij}\,, \qquad (3.1)$$

where α_i and α_j are the deformation parameters, H is the single-particle hamiltonian, u_ν and v_ν are the BCS variational parameters and E_ν is the quasi-particle energy corresponding to the single-particle state $|\nu\rangle$. The term P^{ij} describes the effect of the collective motion on the pairing interaction. Various properties of the tensor $B_{\alpha_i\alpha_j}$ have been discussed in [8–13].

3.3. Deformation space

Main attention is concentrated on the axially symmetric shapes of a nucleus. The effects of non-axial shapes are, however, also discussed.

3.3.1. Axially symmetric shapes

The axially symmetric shapes may be described by the usual deformation parameters β_λ, appearing in the expression for nuclear radius (in the intrinsic frame of reference) in terms of spherical harmonics,

$$R(\vartheta) = R_0(\beta_\lambda)[1 + \sum_\lambda \beta_\lambda Y_{\lambda 0}(\vartheta)]\,, \qquad (3.2)$$

where the dependence of R_0 on β_λ is determined by the volume-conservation condition.

The study performed in the present paper shows that the odd-multipolarity deformations β_λ, $\lambda = 3, 5, \ldots$ do not contribute to the energy of the investigated nucleus $^{260}106$ in any part of the region of its fission barrier. Concerning the even multipolarities, the first four of them, $\lambda = 2, 4, 6, 8$, contribute to the barrier. The contribution of $\lambda = 10$ is already negligible. Thus, the analysis is performed in the 4-dimensional space $\{\beta_\lambda\}$, $\lambda = 2, 4, 6, 8$.

3.3.2. Non-axial shapes

In our study of the effects of non-axial shapes, we include the non-axiality to the shapes described by the most important deformations of the lowest multipolarity degrees: $\lambda = 2$ and 4. A general non-axiality of the quadrupole deformation, $\lambda = 2$, is described by one parameter γ_2, while that of the hexadecapole deformation, $\lambda = 4$, needs two parameters: γ_4 and δ_4 [14]. Here, to have a smaller number of free parameters, we admit (similar as in [15, 16]) a particular hexadecapole non-axial deformation with $\gamma_4 = -2\gamma_2$ and $\delta_4 = \delta_4^0 = \arccos\sqrt{\frac{7}{12}}$ [14]. Then, the whole non-axiality is described by only one parameter γ ($\gamma \equiv \gamma_2$) and the expression for nuclear radius $R(\vartheta, \varphi)$ (in the intrinsic frame of reference) in terms of spherical harmonics $Y_{\lambda\mu}(\vartheta, \varphi)$ is

$$\begin{aligned} R(\vartheta,\varphi) = & R_0(\beta_\lambda,\gamma)\{1 + \beta_2[\cos\gamma Y_{20} + \frac{1}{\sqrt{2}}\sin\gamma(Y_{22} + Y_{2-2})] \\ & + \beta_4[\frac{1}{12}(7 + 5\cos 2\gamma)Y_{40} + \frac{1}{2}\sqrt{\frac{5}{6}}\sin 2\gamma(Y_{42} + Y_{4-2}) \\ & + \frac{1}{12}\sqrt{\frac{35}{2}}(1 - \cos 2\gamma)(Y_{44} + Y_{4-4})] \\ & + \beta_6 Y_{60} + \beta_8 Y_{80}\}\,. \end{aligned} \tag{3.3}$$

This is the same expression as given in [16], except that the (axial) deformation of multipolarity $\lambda = 8$, disregarded in [16], is also included here. The dependence of R_0 on β_λ ($\lambda = 2, 4, 6, 8$) and γ is determined by the volume-conservation condition.

3.4. Spontaneous-fission half-lives

The spontaneous-fission half-life T_{sf} is calculated by the formula (*e.g.* [13])

$$T_{\mathrm{sf}} = \frac{\ln 2}{nP}\,, \tag{3.4}$$

where n is the number of assaults of a nucleus on the fission barrier in unit time and P is the probability of the penetration through the barrier for a given assault. The probability P is obtained in the semiclassical (WKB) approximation

$$P = [1 + \exp 2S(L)]^{-1}\,, \tag{3.5}$$

where the action integral $S(L)$ along a 1-dimensional trajectory L in a multidimensional deformation space is

$$S(L) = \int_{s_1}^{s_2} \left\{\frac{2}{\hbar^2} B_L(s)[V_L(s) - E]\right\}^{\frac{1}{2}} ds\,. \tag{3.6}$$

Here, $V_L(s)$ is the potential energy, $B_L(s)$ is the effective inertia, both along the trajectory L, and E is the energy of a fissioning nucleus. The parameter s specifies the position of a point on the trajectory L, with s_1 and s_2 corresponding to the entrance and exit points of the barrier, *i.e.* to the classical turning points determined by: $V(s) = E$. The effective inertia $B_L(s)$ associated with the fission motion along the trajectory L is

$$B \equiv B_L(s) = \sum_{ij} B_{\alpha_i \alpha_j}(s) \frac{d\alpha_i}{ds} \frac{d\alpha_j}{ds}, \tag{3.7}$$

where $B_{\alpha_i \alpha_j}$ are components of the inertia tensor, Eq. (3.1), and α_i, α_j are the deformation parameters (β_λ or γ).

The dynamical calculation of $T_{\rm sf}$ consists in the search of the (dynamical) fission trajectory $L_{\rm min}$, which minimizes the action integral $S(L)$.

3.5. Details of the calculations

The potential energy and the inertia tensor are calculated microscopically in the following "basic" grid points

$$\beta_2 = \ 0.20\ (0.05)\ 0.70\,, \qquad \beta_4 = -0.05\ (0.05)\ 0.20\,,$$
$$\beta_6 = -0.08\ (0.04)\ 0.08\,, \qquad \beta_8 = -0.04\ (0.04)\ 0.04\,.$$

In the non-axial degree of freedom γ, the "basic" grid points are

$$\sin\gamma = 0\ (0.075)\ 0.30/\beta_2\,.$$

To get the values of all calculated quantities for grid points, which are few times more dense in each degree of freedom, the standard SPLIN3 procedure of the IMSL library has been used for the interpolation (by third order polynomials). Only in the β_8 degree of freedom, the parabolic interpolation has been applied.

4. Results

4.1. Potential energy

To have small values of the energy, we employ, in the whole paper, the usual normalization of the energy, putting the smooth part of the energy equal to zero at the zero deformation. In other words, we subtract from the energy a constant value equal to the smooth part of the energy of a nucleus at its spherical shape. This is reasonable as we are only interested in the

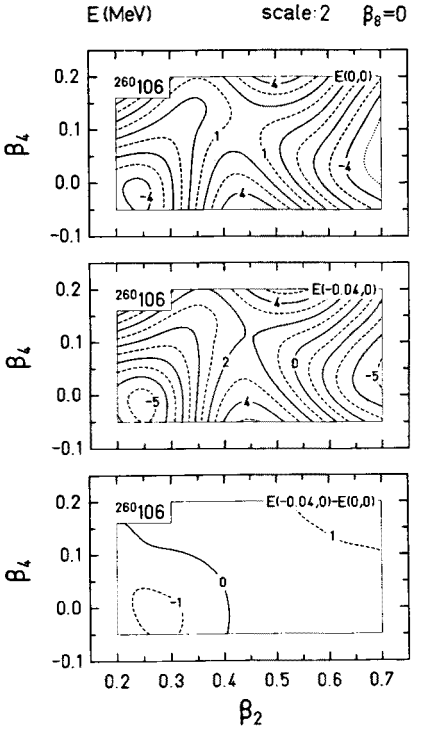

Fig. 3. Contour maps of the potential energy E, plotted as a function of the deformations β_2 and β_4 for $\beta_6 = 0$, $E(0,0)$, and $\beta_6 = -0.04$, $E(-0.04,0)$, both for $\beta_8 = 0$, and the difference between the two. Numbers at the contour lines give the values of the energy in MeV. Difference in the values between neighbouring solid lines is specified by the scale. Dashed lines divide this difference by two.

dependence of the energy on deformation, and not in the absolute value of it.

Fig. 3 illustrates the dependence of the energy on the deformations of the lowest multipolarities, β_2 and β_4, with the deformations β_6 and β_8 treated as parameters. To shorten the notation, we put

$$E(\beta_2, \beta_4; \beta_6, \beta_8) \equiv E(\beta_6, \beta_8)\,. \tag{4.1}$$

The figure shows the energy at $\beta_6 = 0$ and $\beta_6 = -0.04$, and the difference between the two, all with $\beta_8 = 0$. One can see that, at $\beta_6 = 0$, the equilibrium deformation is $\beta_2^0 \approx 0.24$, $\beta_4^0 \approx -0.02$ and the value of the energy is about -4.6 MeV. At $\beta_6 = -0.04$, the position of the minimum remains practically the same, but the energy is lower by about 1 MeV. The position of the saddle point also remains about the same, but the energy is higher by more than 0.5 MeV. Thus, the fission barrier in the $\beta_6 = -0.04$ plane is

higher by more than 1.5 MeV than in the $\beta_6 = 0$ plane. This suggests that the fission trajectory in a multidimensional deformation space, including β_6 as a variable, will have a tendency to start at low, negative value of β_6 and then to proceed towards increasing values of this deformation. This is really the case, as will be seen in Fig. 13. The lowest map of Fig. 3 illustrates more directly the effect of the change of β_6, from $\beta_6 = 0$ to $\beta_6 = -0.04$, on the energy.

4.2. Inertia tensor

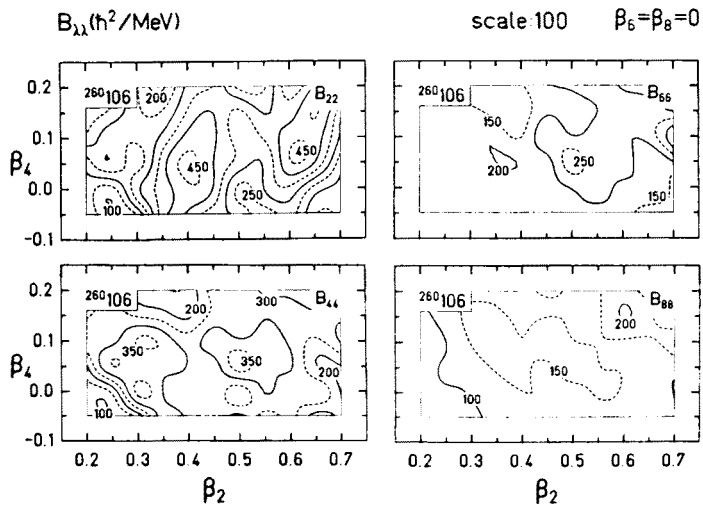

Fig. 4a. Contour maps of the diagonal components $B_{\lambda\lambda}$ ($\lambda = 2, 4, 6, 8$) of the inertia tensor calculated at $\beta_6 = \beta_8 = 0$.

Fig. 4a illustrates the dependence of the diagonal components $B_{\lambda\lambda}$ of the inertia tensor on the deformations β_2 and β_4 at $\beta_6 = \beta_8 = 0$, for $\lambda = 2, 4, 6, 8$. Such illustrations have been given earlier only for 2-dimensional deformation spaces (*e.g.* [11, 13]). To shorten the notation, it is put here

$$B_{\beta_\lambda \beta_\mu} \equiv B_{\lambda\mu}\,. \tag{4.2}$$

One can see in Fig. 4a that $B_{\lambda\lambda}$ are fast fluctuating functions of deformation. The reason is that $B_{\lambda\lambda}$ are not very collective quantities and they sensitively depend on the positions of few pairs of the single-particle levels, which are close to the Fermi level. The largest fluctuations are obtained for the main component of the tensor, B_{22}. Then, the fluctuations of $B_{\lambda\lambda}$ decrease with increasing λ. All components have the smallest values around the point of minimal energy and these values are similar for all λ.

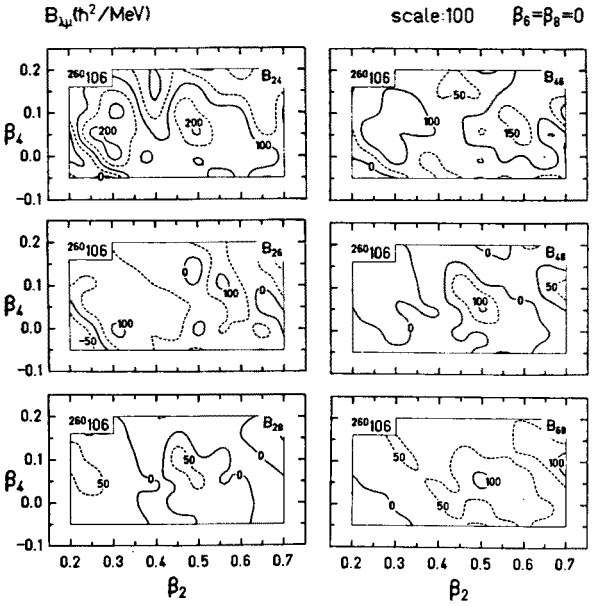

Fig. 4b. Same as in Fig. 4a, but for the non-diagonal components $B_{\lambda\mu}, \mu \neq \lambda$, of the inertia tensor.

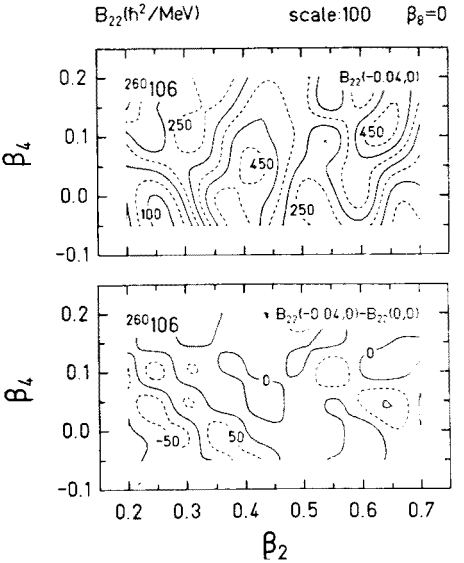

Fig. 5. Contour map of the component B_{22} of the inertia tensor calculated at $\beta_6 = -0.04$ and $\beta_8 = 0$, $B_{22}(-0.04, 0)$, and difference between it and that calculated at $\beta_6 = \beta_8 = 0$, $B_{22}(0, 0)$.

The non-diagonal components $B_{\lambda\mu}$, $\lambda \neq \mu$, are shown in Fig. 4b. One

can see that these components are also much fluctuating with deformation. The largest values are obtained for the main non-diagonal component B_{24}. Values of the other components $B_{\lambda\mu}$ are decreasing with increasing λ and, even more, with increasing $|\lambda - \mu|$. For almost whole investigated region of deformation, the values of non-diagonal components are positive.

Fig. 5 shows how much the map of the main component of the tensor, $B_{22}(\beta_2, \beta_4)$, changes with a change of β_6. Comparing the B_{22} of the upper part of Fig. 5 ($\beta_6 = -0.04$) with that of Fig. 4a ($\beta_6 = 0$), one can see that they are similar. The lower part of Fig. 5 gives directly the difference between the two and shows that the difference is really small. The values of B_{22} at $\beta_6 = -0.04$ are lower by about $50\hbar^2/\text{MeV}$ than at $\beta_6 = 0$, for deformations around the point of minimal energy. This is because this minimal energy is lower at $\beta_6 = -0.04$ than at $\beta_6 = 0$, which means that the density of the single-particle levels around the Fermi level is smaller at $\beta_6 = -0.04$. The lower density of these levels results in the lower values of the inertia function B_{22}.

4.3. Fission trajectory

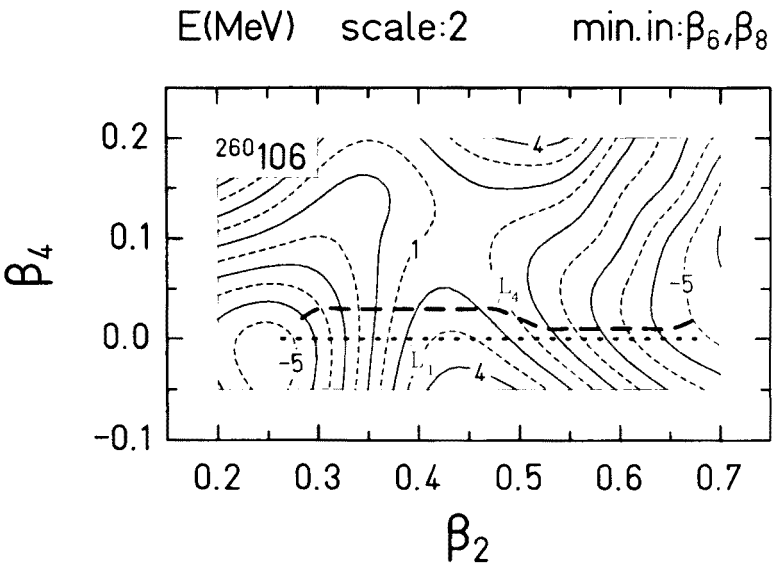

Fig. 6. Fission trajectories L_1 and L_4 obtained in 1- and 4-dimensional deformation spaces.

Fig. 6 shows the (dynamical) fission trajectories L_1 and L_4 obtained in 1- and 4-dimensional deformation spaces $\{\beta_\lambda\}$, $\lambda = 2$ ($\lambda_{\max} = 2$) and $\lambda = 2, 4, 6, 8$ ($\lambda_{\max} = 8$), respectively. Although the trajectories are also

analyzed in 2- and 3-dimensional spaces, only two of them (corresponding to the extreme cases of the dimension of the deformation spaces discussed) are shown, for reason of clarity. To understand the "physics" of the trajectory L_4, we also plot the map of the potential energy. As we cannot, however, plot the potential energy of the 4-dimensional space in this 2-dimensional figure, the "projected" energy is shown. It is the energy which, for each point (β_2, β_4), is minimized in the β_6 and β_8 degrees of freedom. One can see that the dynamical trajectory L_4 passes the potential-energy barrier in such a way as to possibly little change the deformation β_4 of the nucleus. We will see in Fig. 13 that also the deformations β_6 and β_8 are being only little and smoothly changed along the trajectory. Thus, although the trajectory has some tendency to approach the saddle point, which is rather far in the β_4, β_6 and β_8 deformations from the entrance point to the barrier, it passes in some distance from the saddle point, trying to change all the deformations β_λ, other than β_2, as little as possible. Along such trajectory, the effective B_L, Eq. (3.7), and also the action integral $S(L)$, Eq. (3.6), is relatively small.

4.4. Fission barrier

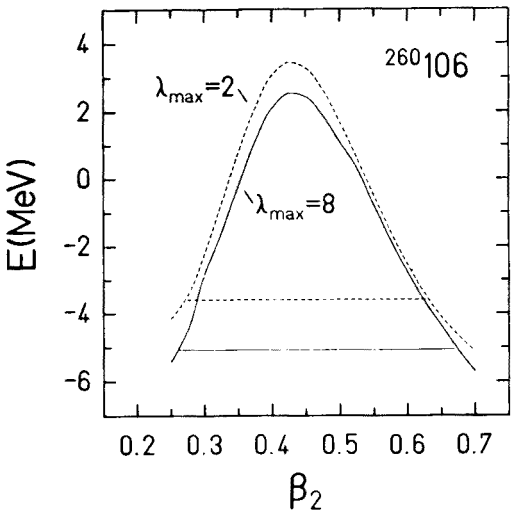

Fig. 7. Fission barriers obtained in 1- ($\lambda_{\max} = 2$) and 4-dimensional ($\lambda_{\max} = 8$) deformation spaces.

Fig. 7 shows the fission barrier obtained in 1- ($\lambda_{\max} = 2$) and 4-dimensional ($\lambda_{\max} = 8$) deformation spaces. This is the potential energy calculated along the trajectories L_1 and L_4 (shown in Fig. 6), respectively. One can see that the barrier obtained in 4-dimensional space is higher and

thicker. This is mainly due to the lower (by about 1.5 MeV) potential energy obtained at the equilibrium (ground state) point in the 4-dimensional case. In both cases, the same zero-point energy (corresponding to the vibration of a nucleus in the fission degree of freedom), equal to 0.7 MeV, is taken, to obtain the ground-state energy (horizontal thin lines) from the minimal value of the potential energy. It is worth mentioning that a large difference between the energies obtained at the top of the two shown barriers is connected with the fact that these energies do not correspond to the same, or even similar, saddle points.

4.5. Effective inertia

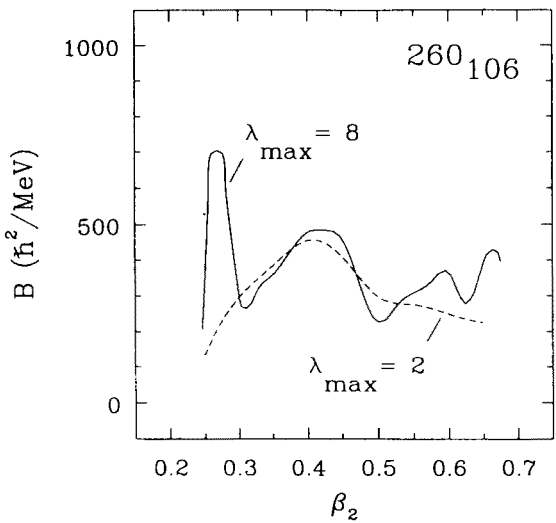

Fig. 8. Same as in Fig. 7, but for the effective inertia B.

Fig. 8 gives the effective inertia B, Eq. (3.7), obtained along the fission trajectories L_1 ($\lambda_{\max} = 2$) and L_4 ($\lambda_{\max} = 8$) shown in Fig. 6. One can see that the inertia is much different in these two cases. This difference, besides the difference in the barrier, gives a contribution to the difference in the fission half-life T_{sf}.

4.6. Fission half-life

Fig. 9 shows logarithm of the spontaneous-fission half-life T_{sf} as a function of the dimension of the deformation space used in the analysis. The dimension is parameterized by the maximal multipolarity, $\lambda_{\max}$, of the deformations taken. One can see that T_{sf} increases with increasing dimension

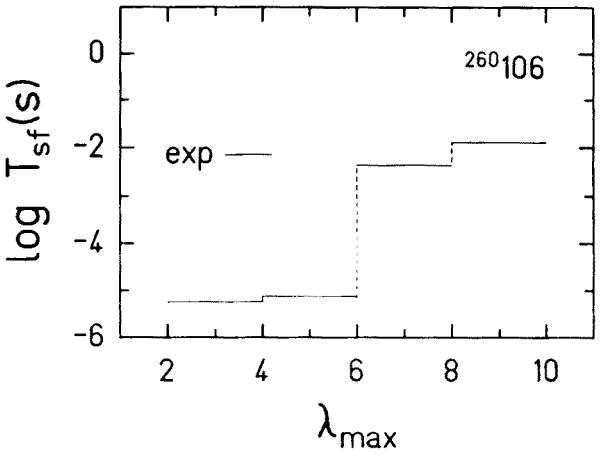

Fig. 9. Logarithm of the spontaneous-fission half-life T_{sf} (given in seconds) as a function of the maximal multipolarity, λ_{max}, of the deformations used. Experimental value of T_{sf} is also shown.

of the space, mainly due to the increase of the fission barrier. In particular, the inclusion of the deformation β_6, usually disregarded or treated approximately, increases T_{sf} by about 3 orders of magnitude. This means that the analysis of T_{sf} of the nucleus $^{260}106$ in the 2-dimensional space $\{\beta_\lambda\}$, $\lambda = 2, 4$, would be much misleading. The use of a more (at least 3)-dimensional spaces seems to be necessary.

5. Discussion

5.1. Analysis in the "projected" space

Dynamical calculation of the fission lifetimes in a large deformation space is a complex and time-consuming task. Thus, one tries to find a way of reducing the dimension of the space as much as possible. A way, however, which does not spoil too much the results.

One of the ways of such reduction is to use, in a smaller space, the potential energy which takes into account the effect of the omitted deformations. Usually, it is the potential energy which, for each point of the smaller space, is minimized in these omitted deformation degrees of freedom. For example, when reducing the 3-dimensional space $\{\beta_\lambda\}$, $\lambda = 2, 4, 6$ to the 2-dimensional one $\{\beta_\lambda\}$, $\lambda = 2, 4$, one takes the potential energy which, for each point (β_2, β_4), is minimized in the β_6 degree of freedom. We will call the smaller space: the "projected" space.

In the present section, effects of reducing the 4-dimensional space $\{\beta_\lambda\}$, $\lambda = 2, 4, 6, 8$, to the space of a lower dimension will be discussed. These are

the effects on the potential energy, fission trajectory, effective inertia and fission lifetime.

5.1.1. Potential energy

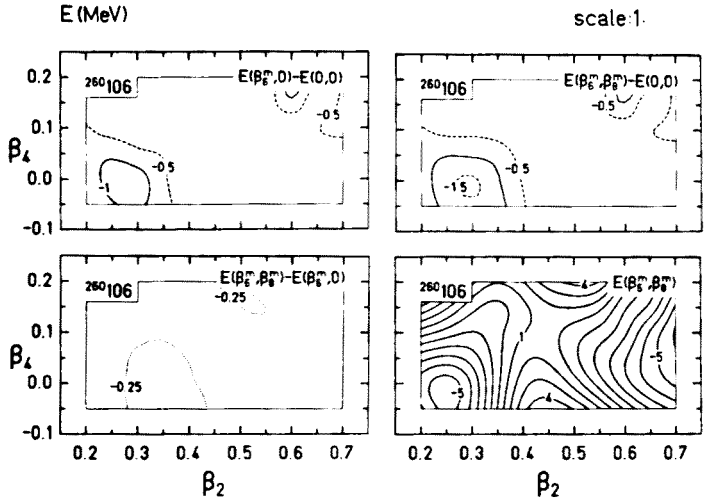

Fig. 10. Effect of minimization of the potential energy in the β_6 and β_8 degrees of freedom, on the values of this energy.

Fig. 10 illustrates the effect of minimization of the potential energy $E(\beta_2, \beta_4; \beta_6, \beta_8)$ in the β_6 and β_8 degrees of freedom. Here, β_λ^m, $\lambda = 6, 8$, denotes the value of β_λ at which the energy is minimal in this degree of freedom. The other notation is the same as in Fig. 3. One can see that the minimization in β_6 lowers the energy mainly in the region around the equilibrium point and that the effect is up to more than 1 MeV. The largest effect of minimization in the deformation β_8 also appears around the equilibrium point, but is smaller, less than 0.5 MeV. Thus, the total effect of minimization in both these degrees of freedom, $E(\beta_6^m, \beta_8^m) - E(0,0)$, is to decrease the energy by up to more than 1.5 MeV. The final plot of the potential energy $E(\beta_6^m, \beta_8^m) \equiv E(\beta_2, \beta_4; \beta_6^m, \beta_8^m)$ in the "projected" space $\{\beta_\lambda\}$, $\lambda = 2, 4$, is shown in the lower right corner of the figure. It is the same plot as already seen in Fig. 6.

5.1.2. Deformations and shapes

Fig. 11 shows the deformations β_6^m and β_8^m for which the energy is minimal. The plots are direct reflections (and *vice versa*) of the plots: $E(\beta_6^m, 0) - E(0,0)$ and $E(\beta_6^m, \beta_8^m) - E(\beta_6^m, 0)$ (Fig. 10) showing the effect of β_6^m and β_8^m on the energy. One can see that the largest values of β_6^m and β_8^m

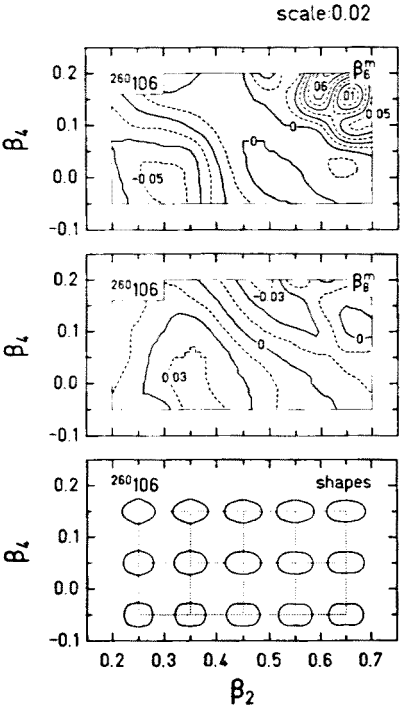

Fig. 11. Contour maps of the deformations β_6^m and β_8^m, at which the potential energy is minimal, and corresponding shapes of the investigated nucleus $^{260}106$.

(in the absolute value) are obtained in the region of the equilibrium point. [Large values of β_6^m and β_8^m are also obtained in the region of large β_2 and β_4, which is rather far from the fission trajectory and,thus, less interesting for the problem discussed here.] In a large part of the deformation region, analyzed here, β_6^m and β_8^m are small, close to zero. In the lower part of the figure, the shapes of the nucleus corresponding to these deformations are illustrated.

5.1.3. Inertia tensor

Fig. 12 illustrates the effect of inclusion of the deformations β_6 and β_8 on the main component of the inertia tensor B_{22}. The effect is obtained by calculating B_{22}, for each point of the smaller space $\{\beta_\lambda\}$, $(\lambda = 2, 4)$, at the deformations β_6^m and β_8^m which minimize the potential energy in β_6 and β_8 at that point. Thus, the figure is done in full analogy to Fig. 10, prepared for the potential energy.

One can see that the effect is rather small, especially that of the deformation β_8. The final effect is to decrease B_{22} by about $50\hbar^2/\mathrm{MeV}$ around the equilibrium point and to increase it by about the same value in an-

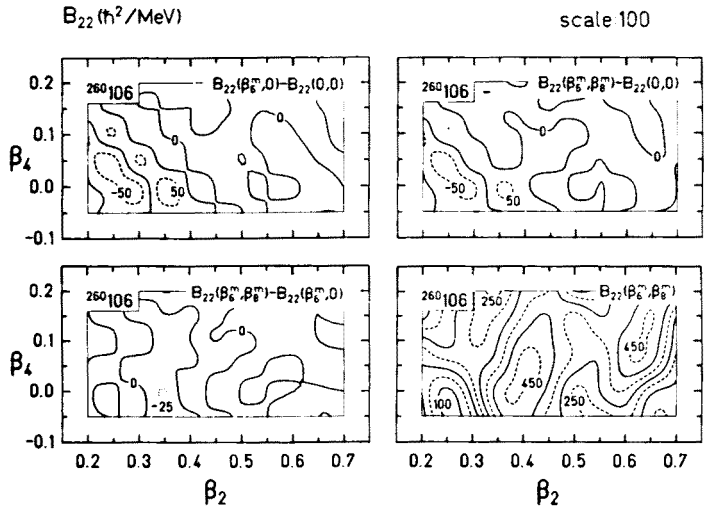

Fig. 12. Same as in Fig. 10, but for the main component of the inertia tensor B_{22}.

other region of deformations. The mechanism of the decrease around the equilibrium point is the same as for the potential energy. The decrease of both quantities comes from the decrease of the density of the single-particle levels, close to the Fermi level, due to the inclusion of additional degrees of freedom in minimization of the potential energy.

5.1.4. Fission trajectory

Three kinds of the fission trajectory are shown in Fig. 13. One (L_4) is the dynamical trajectory obtained in the full 4-dimensional deformation space $\{\beta_\lambda\}$, $\lambda = 2,4,6,8$. This is the same trajectory (L_4) as shown already in Fig. 6. In that figure, it has been illustrated, however, only in the (β_2,β_4) plane, while here it is also given in the (β_2,β_6) and (β_2,β_8) planes. The second trajectory (L_{2p}) is obtained dynamically in the projected 2-dimensional space $\{\beta_\lambda\}$ ($\lambda = 2,4$), *i.e.* with the potential energy (shown in Fig. 6 and also in lower right corner of Fig. 10), which is minimized in β_6 and β_8 deformations, and with the inertia tensor $B_{\lambda\mu}$ calculated with $\beta_6 = \beta_6^m$ and $\beta_8 = \beta_8^m$ in each point (β_2,β_4). The third trajectory (L_s) is the static trajectory, *i.e.* the line along which, for each β_2, the energy is minimized in all other deformations.

It is rather easy to understand the shape of the trajectories. The shape of the static trajectory is directly dictated by the potential energy and can be easily "read" from a plot of this energy in a given plane (β_2,β_λ). The dynamical trajectory has a tendency to proceed in such a way as to possibly little and smoothly change any deformation β_λ ($\beta_\lambda \neq \beta_2$) of a nucleus. In such case, the contribution of the components of the inertia tensor $B_{\lambda\mu}$ to

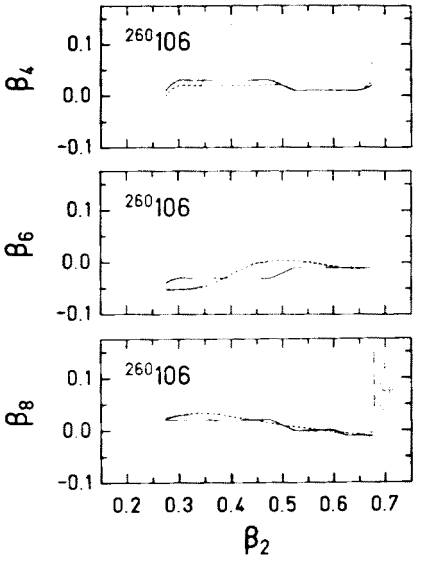

Fig. 13. Three kinds of the fission trajectory: dynamical one obtained in 4-dimensional space (L_4), dynamical trajectory obtained in 2-dimensional projected space (L_{2p}) and the static trajectory (L_s).

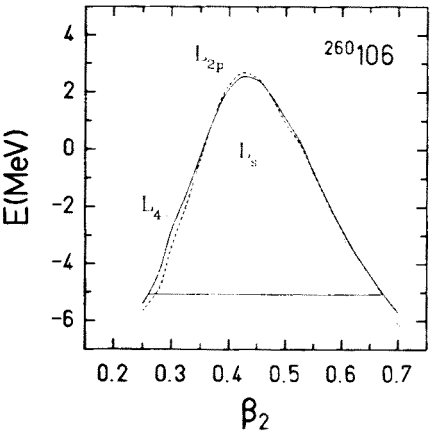

Fig. 14. Fission barrier along the three fission trajectories (L_4, L_{2p} and L_s) shown in Fig. 13.

the effective inertia B is small (as $d\beta_\lambda/d\beta_2$ is small, see Eq. (3.7)) and the inertia B and, thus, the action integral, Eq. (3.6), are relatively small. If the potential energy forces a change in the deformation β_λ of a nucleus, it is the most "economic" for it to make this change in the region around the beginning or the end of the fission barrier, where the potential energy is small and a large inertia B is of relatively small importance for the value

of the action integral. In a more "microscopic" language, a small change of β_λ means a small change of the internal structure of a nucleus and, thus, also a small inertia or "resistance" of it to this change.

One can see in Fig. 13 that the trajectory L_4, obtained dynamically in the whole 4-dimensional space, is horizontal (independent of β_λ, $\lambda = 4, 6, 8$) in a large part of the region inside the fission barrier, which means a relatively small effective inertia. The trajectory L_{2p} is close to it only in the (β_2, β_4) plane, *i.e.* in the plane in which it has also been obtained dynamically.

5.1.5. Fission barrier

Fig. 14 gives the fission barrier calculated along the three fission trajectories shown in Fig. 13. One can see that the two dynamical barriers (one obtained in full 4-dimensional space and the other in the projected 2-dimensional space) are close to each other. This is because the respective trajectories are close to each other in the main degrees of freedom: β_2 and β_4. The static barrier differs much from the two dynamical barriers, especially in the region around the saddle point. It is lower than these two barriers by more than 1 MeV.

5.1.6. Effective inertia

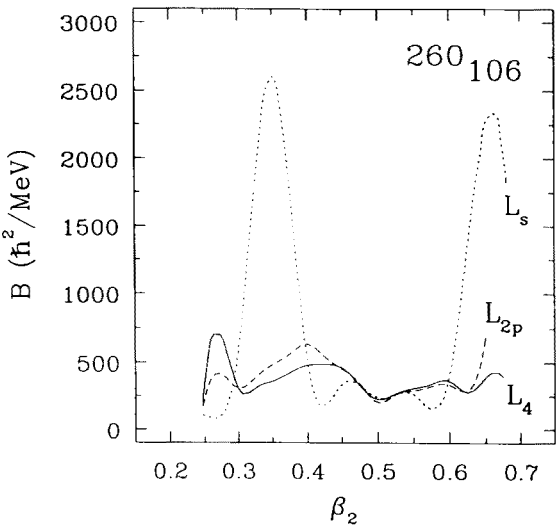

Fig. 15. Same as in Fig. 14, but for the effective inertia of the nucleus $^{260}106$.

Fig. 15 shows the effective inertia B calculated along the three trajectories: L_4, L_{2p} and L_s given in Fig. 13. One can see that the inertia

is generally lowest along the dynamical trajectory L_4, what should be expected according to the discussion of subsect. 5.1.4. Large values of it, observed at the beginning of the barrier, have rather small influence on the action integral, as also discussed in subsect. 5.1.4.

The inertia obtained along the static trajectory L_s has two large maxima, one of them appearing in the region ($\beta_2 \approx 0.35$) of a large potential energy and, thus, having important influence on the value of the action integral and, through it, on the fission half-life. This maximum is directly connected with a fast change of the deformation β_4 along L_s in this region of the deformation β_2 (see Fig. 13). This fast change of β_4 results in a large contribution of the component B_{44} of the inertia tensor to the effective inertia B. This contribution is about four times larger, in the region of the maximum, than the contribution of B_{22} which is usually the most important.

5.1.7. Fission half-life

The dynamical calculation of the spontaneous-fission half-life T_{sf}, performed in the full 4-dimensional space (*i.e.* along the trajectory L_4, Fig. 13), leads to $\log_{10} T_{sf}(s) = -1.89$. The dynamical calculation done in the projected 2-dimensional space (*i.e.* along the trajectory L_{2p}) gives a rather close value: $\log_{10} T_{sf}(s) = -1.76$. The calculation performed along the static trajectory L_s gives: $\log_{10} T_{sf}(s) = 0.75$, *i.e.* the half-life by about 2.6 orders of magnitude larger than along L_4. This is due to large inertia B along this trajectory, as illustrated in the previous subsection.

5.2. Effect of non-axial deformations

Fig. 16 shows the dependence of the potential energy on the non-axiality parameter γ, defined by Eq. (3.3). Here, the line $\gamma = 0$ represents a trajectory in the 4-dimensional deformation space $\{\beta_\lambda\}$ ($\lambda = 2, 4, 6, 8$) which is not far from the dynamical trajectory L_4. The position of a point on this trajectory is described by the deformation β_2. The deformations β_λ ($\lambda = 4, 6, 8$) along the trajectory are functions of β_2. At any point (β_2, γ) on the plane, these deformations β_λ are taken the same as in the point $(\beta_2, 0)$ on the $\gamma = 0$ line.

One can see that the static trajectory (not shown explicitly in Fig. 16) starts at the line $\gamma = 0$, passes through the saddle point with a $\gamma \neq 0$ and comes back to the $\gamma = 0$ line. The energy at the saddle point is by about 1 MeV lower than the energy at the top of the barrier along the $\gamma = 0$ line. Still, the dynamical calculations shows that the dynamical trajectory is very close to the $\gamma = 0$ line. The lifetime T_{sf} along this trajectory is only by about 0.03 orders of magnitude shorter than along the line $\gamma = 0$. In

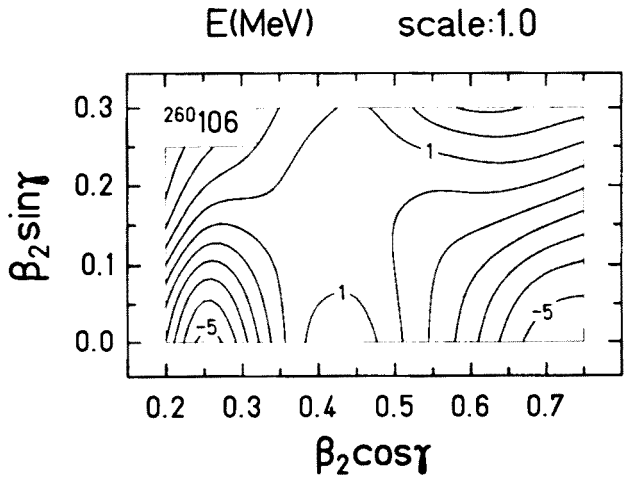

Fig. 16. Dependence of the potential energy E on the non-axial deformation γ.

other words, the effect of the γ degree of freedom on the (dynamical) T_{sf} is very small. This result is similar to that of [17], calculated for a lighter nucleus.

We would like to thank J. Skalski for an important contribution to this study and P. Armbruster, S. Hofmann, G. Münzeberg, W. Nörenberg and Z. Patyk for helpful discussions and suggestions.

REFERENCES

[1] Z. Patyk, A. Sobiczewski, P. Armbruster, K.-H. Schmidt, *Nucl. Phys.* **A491**, 267 (1989).
[2] A. Sobiczewski, Z. Patyk, S. Ćwiok, P. Rozmej, *Nucl. Phys.* **A485**, 16 (1988).
[3] Z. Patyk, A. Sobiczewski, *Nucl. Phys.* **A533**, 132 (1991).
[4] R. Smolańczuk, J. Skalski, H.V. Klapdor-Kleingrothaus, A. Sobiczewski, *Proc. 27th Zakopane School of Physics*, eds. R. Broda and Z. Stachura, Kraków 1993, in press.
[5] H.J. Krappe, J.R. Nix, A.J. Sierk, *Phys. Rev.* **C20**, 992 (1979).
[6] P. Möller, J.R. Nix, *Nucl. Phys.* **A361**, 117 (1981); *At. Data Nucl. Data Tables* **26**, 165 (1981).
[7] S. Ćwiok, J. Dudek, W. Nazarewicz, J. Skalski, T. Werner, *Comput. Phys. Commun.* **46**, 379 (1987).
[8] A. Sobiczewski, Z. Szymański, S. Wycech, S.G. Nilsson, J.R. Nix, C.F. Tsang, P. Möller, B. Nilsson, *Nucl. Phys.* **A131**, 67 (1969).
[9] M. Brack, J. Damgaard, A.S. Jensen, H.C. Pauli, V.M. Strutinsky, C.Y. Wong, *Rev. Mod. Phys.* **44**, 320 (1972).

[10] H.C. Pauli, *Phys. Reports* **7C**, 35 (1973); *Nucleonika* **20**, 601 (1975).
[11] K. Pomorski, T. Kaniowska, A. Sobiczewski, S.G. Rohoziński, *Nucl. Phys.* **A283**, 394 (1977).
[12] A. Sobiczewski, *Sov. J. Part. and Nuclei* **10**, 1170 (1979).
[13] A. Baran, K. Pomorski, A. Łukasiak, A. Sobiczewski, *Nucl. Phys.* **A361**, 83 (1981).
[14] S.G. Rohoziński, A. Sobiczewski, *Acta Phys. Pol.* **B12**, 1001 (1981).
[15] K. Böning, Z. Patyk, A. Sobiczewski, S. Ćwiok, *Z. Phys.* **A325**, 479 (1986).
[16] S. Ćwiok, A. Sobiczewski, *Z. Phys.* **A342**, 203 (1992).
[17] A. Baran, K. Pomorski, S.E. Larsson, P. Möller, S.G. Nilsson, J. Randrup, A. Sobiczewski, *Proc. 3rd Int. Conf. on nuclei far from stability*, Cargèse 1976, CERN 76-13, Geneva, 1976, p.537.